

# Zeeman spin-orbit coupling and magnetic quantum oscillations in antiferromagnetic conductors

R. Ramazashvili,<sup>1,\*</sup> P. D. Grigoriev,<sup>2,3,4,†</sup> T. Helm,<sup>5,6,‡</sup> F. Kollmannsberger,<sup>5,6</sup> M. Kunz,<sup>5,6,§</sup> W. Biberacher,<sup>5</sup> E. Kampert,<sup>7</sup> H. Fujiwara,<sup>8</sup> A. Erb,<sup>5,6</sup> J. Wosnitzer,<sup>7,9</sup> R. Gross,<sup>5,6,10</sup> and M. V. Kartsovnik<sup>5,¶</sup>

<sup>1</sup>*Laboratoire de Physique Théorique, Université de Toulouse, CNRS, UPS, France*

<sup>2</sup>*L. D. Landau Institute for Theoretical Physics, 142432 Chernogolovka, Russia*

<sup>3</sup>*National University of Science and Technology MISiS, 119049 Moscow, Russia*

<sup>4</sup>*P.N. Lebedev Physical Institute, 119991 Moscow, Russia*

<sup>5</sup>*Walther-Meißner-Institut, Bayerische Akademie der Wissenschaften,  
Walther-Meißner-Strasse 8, D-85748 Garching, Germany*

<sup>6</sup>*Physik-Department, Technische Universität München, D-85748 Garching, Germany*

<sup>7</sup>*Hochfeld-Magnetlabor Dresden (HLD-EMFL) and Würzburg-Dresden Cluster of Excellence ct.qmat,  
Helmholtz-Zentrum Dresden-Rossendorf, 01328 Dresden, Germany*

<sup>8</sup>*Department of Chemistry, Graduate School of Science,  
Osaka Prefecture University, Osaka 599-8531, Japan*

<sup>9</sup>*Institut für Festkörper- und Materialphysik, TU Dresden, 01062 Dresden, Germany*

<sup>10</sup>*Munich Center for Quantum Science and Technology (MCQST), D-80799 Munich, Germany*

(Dated: August 6, 2019)

We find that the Néel state of the layered organic conductor  $\kappa$ -(BETS)<sub>2</sub>FeBr<sub>4</sub> shows no spin modulation of the Shubnikov-de Haas oscillations, contrary to the paramagnetic state of the same material. This is evidence of spin degeneracy of Landau levels – a direct manifestation of the generic Zeeman spin-orbit coupling, predicted for antiferromagnetic conductors. Likewise, we find no spin modulation in the angle dependence of the slow Shubnikov-de Haas oscillations in the optimally electron-doped cuprate Nd<sub>2-x</sub>Ce<sub>x</sub>CuO<sub>4</sub>. This points to the presence of Néel order in this superconductor even at optimal doping.

*Introduction* — Spin-orbit coupling (SOC) in solids intertwines electron orbital motion with its spin, generating a variety of fundamental effects [1, 2]. Commonly, SOC originates from the Pauli term  $\mathcal{H}_{\mathcal{P}} = \frac{\hbar}{4m_0^2} \boldsymbol{\sigma} \cdot \mathbf{p} \times \nabla V(\mathbf{r})$  in the electron Hamiltonian [3, 4]. Remarkably, Néel order may give rise to SOC of an entirely different nature, via the Zeeman effect [5, 6]:

$$\mathcal{H}_{\mathcal{Z}}^{so} = -\frac{\mu_B}{2} [g_{\parallel}(\mathbf{B}_{\parallel} \cdot \boldsymbol{\sigma}) + g_{\perp}(\mathbf{k})(\mathbf{B}_{\perp} \cdot \boldsymbol{\sigma})], \quad (1)$$

where  $\mu_B = \frac{e\hbar}{2m_0}$  is the Bohr magneton,  $\mathbf{B}$  the magnetic field,  $\boldsymbol{\sigma}$  the electron spin, while  $g_{\parallel}$  and  $g_{\perp}$  define the  $g$ -tensor components with respect to the Néel axis. In a purely transverse field  $\mathbf{B}_{\perp}$ , a hidden symmetry of a Néel antiferromagnet protects double degeneracy of Bloch eigenstates at a special set of momenta in the Brillouin zone [5, 6]: at such momenta,  $g_{\perp}$  must vanish. The scale of  $g_{\perp}$  is set by  $g_{\parallel}$ , which renders  $g_{\perp}(\mathbf{k})$  substantially momentum-dependent, and turns  $\mathcal{H}_{\mathcal{Z}}^{so}$  into a veritable SOC [5–8]. This coupling may manifest itself in a variety of antiferromagnetic (AF) conductors such as chromium, cuprates, iron pnictides, hexaborides, borocarbides, as well as organic and heavy-fermion compounds [6].

The peculiar form of Eq. (1) is predicted to produce unusual effects such as the absence of Zeeman splitting of the Landau levels in a purely transverse field  $\mathbf{B}_{\perp}$  [9, 10], and spin-flip transitions, induced by AC *electric* rather than magnetic field [10]. To our knowledge, none of these effects have been experimentally verified as yet.

Here we report experimental evidence for the absence

of Zeeman splitting of Landau levels in an AF metal. We examine two very different layered conductors: the organic AF charge-transfer salt  $\kappa$ -(BETS)<sub>2</sub>FeBr<sub>4</sub> (hereafter  $\kappa$ -BETS) [11] and the electron-doped cuprate superconductor Nd<sub>2-x</sub>Ce<sub>x</sub>CuO<sub>4</sub> (NCCO) [12], focusing on the angular dependence of the Shubnikov-de Haas (SdH) oscillations, a sensitive technique for quantifying the Zeeman effect [13].

We find that in both materials the SdH amplitude decreases monotonically with tilting the field away from the normal to conducting layers: remarkably, the oscillations are *not* modulated by the Zeeman splitting. We show that for the organic conductor such a behavior is a natural consequence of the commensurate Néel order giving rise to the Zeeman SOC in the form of Eq. (1).

Both in optimally doped NCCO [14] and in  $\kappa$ -BETS [15], the slow SdH oscillations are associated with a Fermi surface reconstruction, caused by a commensurate order. However, in NCCO the nature of the order remains controversial [12, 16–20]. Our findings provide firm evidence that this state involves Néel order. Note that, contrary to YBa<sub>2</sub>Cu<sub>3</sub>O<sub>6.5+ $\delta$</sub> , where the analysis of earlier experiments [21, 22] was complicated by the bilayer splitting of the Fermi cylinder [22], the single-layer structure of NCCO poses no such difficulty.

Before presenting the experimental results, let us recapitulate the effect of Zeeman splitting on quantum oscillations. In both materials at hand, the electron dispersion is highly anisotropic, allowing us to treat it as two-dimensional (2D). Then, up to a constant, the

phase  $\varphi$  of the first quantum oscillation harmonic is  $\varphi = \frac{F}{B} = \frac{\hbar}{e} \frac{\mathcal{F}}{B \cos \theta}$ , where  $F$  denotes the oscillation frequency,  $\mathcal{F}$  the area enclosed by the Fermi surface,  $B$  the magnetic field, and  $\theta$  the tilt angle between the field and the normal to the conducting plane. The Zeeman effect splits the degenerate Fermi surface, breaking up  $\mathcal{F}$  into  $\mathcal{F}_+$  and  $\mathcal{F}_-$ , with  $\delta\mathcal{F} = \mathcal{F}_+ - \mathcal{F}_- \propto B$ . Adding the two harmonic oscillations at close frequencies  $F_+$  and  $F_-$  is equivalent to a single oscillation at frequency  $F$ , with an amplitude modulated by the spin reduction factor

$$R_s(\theta) = \cos \left[ \frac{\hbar}{2e} \frac{\delta\mathcal{F}}{B \cos \theta} \right]. \quad (2)$$

The experiments were performed in a purely transverse field  $\mathbf{B}_\perp$ . In this case, Eq. (1) defines the Zeeman-split Fermi surfaces via  $\mathcal{E}_\pm(\mathbf{k}) = \mathcal{E}(\mathbf{k}) \pm \frac{1}{2} \mu_B g_\perp(\mathbf{k}) B_\perp$ , where  $\mathcal{E}(\mathbf{k})$  is the zero-field carrier dispersion. Calculating  $\delta\mathcal{F}$  to linear order in  $B_\perp$  allows us to recast Eq. (2) as

$$R_s(\theta) = \cos \left[ \frac{\bar{g}_\perp m}{2m_0} \frac{\pi}{\cos \theta} \right], \quad (3)$$

with the cyclotron mass  $m$  and  $\bar{g}_\perp$  defined by

$$2\pi m = \oint_{FS} \frac{dk}{|\nabla_{\mathbf{k}} \mathcal{E}(\mathbf{k})|}, \quad \bar{g}_\perp = \oint_{FS} \frac{dk}{2\pi m} \frac{g_\perp(\mathbf{k})}{|\nabla_{\mathbf{k}} \mathcal{E}(\mathbf{k})|}, \quad (4)$$

and the integration performed along the Fermi surface (see Supplemental Material (SM) [23]). For a momentum-independent  $g_\perp(\mathbf{k}) = \text{const}$ , Eq. (3) matches the textbook expression [13] for the spin reduction factor in two dimensions. For non-zero  $\bar{g}_\perp$ , Eq. (3) yields  $R_s(\theta) = 0$  at special values of  $\theta$  called ‘spin-zeros’. The latter provide information about the ratio of the product  $\bar{g}_\perp m$  to its free-electron value  $2m_0$ . This was appreciated early on and used to study materials from elemental metals [13] to layered organic conductors [29–33].

In an antiferromagnet, the Fermi surface is often centered at a point  $\mathbf{k}^*$ , where the equality  $g_\perp(\mathbf{k}^*) = 0$  is protected by symmetry [10] – as it is for  $\kappa$ -BETS [23]. Such a point  $\mathbf{k}^*$  belongs to a line of zeros  $g_\perp(\mathbf{k}) = 0$  crossing the Fermi surface. Hence,  $g_\perp(\mathbf{k})$  changes sign along the Fermi surface, and  $\bar{g}_\perp$  in Eqs. (3) and (4) vanishes by symmetry of  $g_\perp(\mathbf{k})$ . Therefore,  $\delta\mathcal{F} = 0$ : the two Zeeman-split branches of the Fermi surface have equal areas, and the Landau levels undergo no Zeeman splitting. Consequently, the quantum oscillation amplitude is predicted to have no spin-zeros whatsoever [9]. For pockets with Fermi wave vector  $k_F$  well below the inverse AF coherence length  $1/\xi$ ,  $g_\perp(\mathbf{k})$  can be described by the leading term of its expansion in  $\mathbf{k}$ . For such pockets, the present result was obtained in Refs. [9, 10, 34]. According to our estimates [23], both in  $\kappa$ -BETS and in optimally ( $x = 0.15$ ) doped NCCO, the product  $k_F \xi$  considerably exceeds unity; thus, one has to employ the analysis above, apt for a large Fermi surface. The conclusion remains the same:  $\bar{g}_\perp = 0$  [23], see also [35]. With this understanding, let us turn to the experiment.

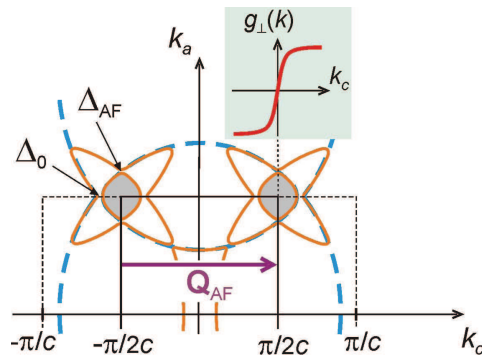


FIG. 1: 2D Fermi surface of  $\kappa$ -BETS, shown in the upper half of the Brillouin zone. The Brillouin zone boundaries in the AF state with the wave vector  $\mathbf{Q}_{\text{AF}} = (\pi/c, 0)$  and in the normal paramagnetic state are shown by solid-black and dashed-black lines, respectively. The dashed blue and solid orange lines show, respectively, the original and reconstructed Fermi surfaces [15]. The shaded area in the corner of the magnetic Brillouin zone, separated from the rest of the Fermi surface by gaps  $\Delta_0$  and  $\Delta_{\text{AF}}$ , is the  $\delta$  pocket responsible for the SdH oscillations observed in the AF state. The inset shows the behavior of  $g_\perp(\mathbf{k})$ , an odd function of  $k_c - \pi/2c$ .

*Antiferromagnetic Organic Superconductor  $\kappa$ -(BETS)<sub>2</sub>FeBr<sub>4</sub>* — This is a quasi-2D metal with conducting layers of the BETS donor molecules, sandwiched between insulating  $\text{FeBr}_4^-$ -anion layers [11]. The material has a centrosymmetric orthorhombic crystal structure (space group  $Pnma$ ), with the  $ac$  plane conventionally chosen along the layers. The Fermi surface is typical of the  $\kappa$ -type salts: it consists of a weakly-warped cylinder and a pair of open sheets, separated from the cylinder by a small gap  $\Delta_0$  at the Brillouin zone boundary, as shown in Fig.1 [11, 36]. Magnetic properties of the compound are mainly governed by five localized  $3d$ -electron spins per  $\text{Fe}^{3+}$  ion in the insulating layers. At temperatures above  $T_N \approx 2.5\text{K}$ , these  $S = 5/2$  spins form a paramagnetic state. Below  $T_N$ , the system develops Néel order with the unit cell doubling along the  $c$  axis and the staggered magnetization pointing along the  $a$  axis [11, 37]. Above a critical magnetic field  $B_c \sim 2 - 5\text{T}$ , depending on the field orientation, the ordering is suppressed, giving way to a saturated paramagnetic state [38].

The Shubnikov-de Haas (SdH) oscillations in the high-field paramagnetic state and in the Néel state are markedly different. In the former, two dominant frequencies corresponding to a classical orbit  $\alpha$  on the Fermi cylinder and to a large magnetic breakdown (MB) orbit  $\beta$  are found, in agreement with the predicted Fermi surface [15, 36] in Fig. S5 of SM [23]. The oscillation amplitude is modulated as a function of the field strength and orientation. This modulation is fairly well described by a field-dependent spin reduction factor  $R_s(\theta, B)$  with the  $g$ -factor  $g = 2.0 \pm 0.2$  in the presence of an exchange

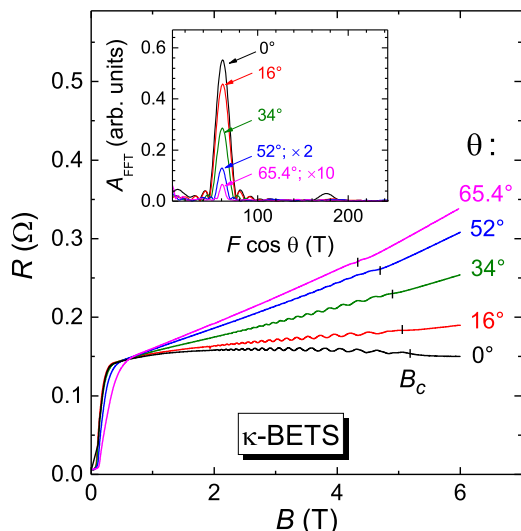


FIG. 2: Examples of the  $B$ -dependent interlayer resistance of  $\kappa$ -BETS at different field orientations, at  $T = 0.42$  K. The AF-paramagnetic transition field  $B_c$  is marked by vertical dashes. Inset: the corresponding FFT spectra of the oscillating magnetoresistance component in the field window 3.0 – 4.2 T. The FFT amplitudes at  $\theta = 52^\circ$  and  $65.4^\circ$  are multiplied by a factor of 2 and 10, respectively.

field  $B_J \approx -13$  T, imposed by paramagnetic  $\text{Fe}^{3+}$  ions on conduction electrons [33, 39].

Below  $B_c$ , in the AF state, the  $\alpha$  and  $\beta$  oscillations disappear, and slow oscillations at the frequency  $F_\delta \approx 62$  T emerge in their stead, indicating a Fermi surface reconstruction [15]. The latter is associated with the folding of the original Fermi surface into the magnetic Brillouin zone, and  $F_\delta$  is attributed to a small, nearly circular orbit  $\delta$ , centered at its corner as shown in Fig. 1. The orbit  $\delta$  emerges due to the gap  $\Delta_{\text{AF}}$  induced by the Néel order at the Fermi surface points, separated by the ordering wave vector  $(0, 0, \pi/c)$  [40].

Figure 2 shows examples of the field-dependent interlayer resistance of  $\kappa$ -BETS recorded at  $T = 0.42$  K, at different tilt angles  $\theta$ . The field was rotated in the plane normal to the Néel axis (crystallographic  $a$  axis). All the curves have a clear feature at the transition between the low-field AF and high-field paramagnetic states. The transition field  $B_c$  gradually decreases with increasing  $\theta$ . In excellent agreement with the previous reports [15, 41], slow oscillations at frequency  $F_\delta = 61.2 \text{ T}/\cos\theta$  are observed below  $B_c$ . Thanks to high crystal quality, even in this low-field region of the phase diagram the  $\delta$  oscillations can be traced in a wide range of tilt angles  $|\theta| \leq 70^\circ$ .

The angular dependence of the SdH amplitude  $A_\delta$  is shown in Fig. 3. The amplitude was determined by the fast Fourier transform (FFT) of the zero-mean oscillating magnetoresistance component normalized to the monotonic background, in a field window of 3.0 to 4.2 T so as to stay in the AF state for all field orientations. The FFT

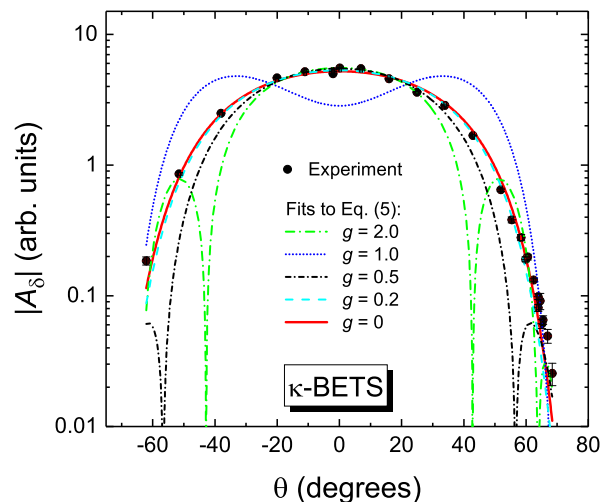


FIG. 3: Angular dependence of the SdH amplitude  $A_\delta$  in the AF state of  $\kappa$ -BETS. The lines are fits to Eq. (5) with different values of the  $g$ -factor.

spectra contain no resolvable higher harmonics of  $F_\delta$ , see inset in Fig. 2. For  $\theta = 0^\circ$ , a small peak at  $F_c \approx 180$  T is resolved and attributed to a larger orbit on the complex reconstructed Fermi surface [41]. The magnitude of this peak falls below the noise level at  $|\theta| \geq 10^\circ$ . Thus, we restrict our analysis to the fundamental harmonic of the  $\delta$  oscillations. The lines in Fig. 3 are fits using the Lifshitz-Kosevich formula for the SdH amplitude [13]:

$$A_\delta = A_0 \frac{m^2}{\sqrt{B}} R_{\text{MB}} \frac{\exp(-KmT_D/B)}{\sinh(KmT/B)} R_s(\theta), \quad (5)$$

where  $A_0$  is a field-independent prefactor,  $B = 3.5$  T (the midpoint of the FFT window in the  $1/B$  scale),  $m = 1.1m_0/\cos\theta$  the effective cyclotron mass [15],  $K = 2\pi^2 k_B/\hbar e$ ,  $T = 0.42$  K,  $T_D$  the Dingle temperature, and  $R_{\text{MB}}$  the MB factor. For  $\kappa$ -BETS,  $R_{\text{MB}}$  takes the form  $R_{\text{MB}} = [1 - \exp(-\frac{B_0}{B \cos\theta})][1 - \exp(-\frac{B_{\text{AF}}}{B \cos\theta})]$  with two characteristic MB fields  $B_0$  and  $B_{\text{AF}}$ , associated with the gaps  $\Delta_0$  and  $\Delta_{\text{AF}}$ , respectively. The Zeeman splitting effect is encapsulated in the spin factor  $R_s(\theta)$ . In Eq. (1), the geometry of our experiment implies  $\mathbf{B}_\parallel = 0$ , thus in the Néel state  $R_s(\theta)$  takes the form of Eq. (3).

Excluding  $R_s(\theta)$ , the other factors in Eq. (5) lead to a monotonic decrease of  $A_\delta$  with increasing  $\theta$ . By contrast,  $R_s(\theta)$  in Eq. (3), generally, has an oscillating angular dependence. For  $\bar{g}_\perp = g = 2.0$  found in the high-field paramagnetic state [33], Eq. (3) yields two spin-zeros, at  $\theta \approx 43^\circ$  and  $\theta \approx 64^\circ$ . Contrary to this, we observe *no* spin-zeros, but rather a monotonic decrease of  $A_\delta$  by over two orders of magnitude as the field is tilted away from  $\theta = 0^\circ$  to  $\theta \approx \pm 70^\circ$ , i.e., in the entire angular range where we observe the oscillations. The different curves in Fig. 3 are our fits to Eq. (5) using  $A_0$  and  $T_D$  as fit parameters, and different values of the  $g$ -factor. We used

the MB field values  $B_0 = 20$  T and  $B_{AF} = 5$  T, which yielded  $T_D \simeq 0.6 \pm 0.1$  K. While the exact values of  $B_0$  and  $B_{AF}$  are unknown, they have virtually no effect on the fit quality [23].

Comparison of the curves in Fig. 3 with the data points shows that the data are incompatible with  $\bar{g}_\perp > 0.2$ . Given the experimental error bars, we cannot rule out a finite  $\bar{g}_\perp \lesssim 0.2$ , yet even such a small finite value would be in stark contrast with the textbook  $g = 2.0$ , found from the SdH oscillations in the high-field, paramagnetic state [33]. Below we argue that, in fact,  $\bar{g}_\perp$  in the Néel state is *exactly* zero.

*Optimally doped NCCO* — This material belongs to the family of electron-doped cuprate superconductors  $Ln_{2-x}Ce_xCuO_4$ , where  $Ln$  stands for La, Nd, Pr, or Sm [12]. All these compounds share a body-centered tetragonal crystal structure (space group  $I4/mmm$ ), where (001) conducting  $CuO_2$  layers alternate with their insulating  $(Ln,Ce)O_2$  counterparts. Band structure calculations [42, 43] predict a hole-like cylindrical Fermi surface, centered at the corner of the Brillouin zone. However, angle-resolved photoemission spectroscopy (ARPES) [44–47] reveals a reconstruction of this Fermi surface by a  $(\pi, \pi)$ -periodic order. Moreover, magnetic quantum oscillation experiments [49–51] show that the Fermi surface remains reconstructed even in the overdoped regime, up to the critical doping  $x_c$  ( $\approx 0.175$  for NCCO), where the superconductivity vanishes [52]. The origin of this reconstruction remains unclear: while the  $(\pi, \pi)$  periodicity is compatible with the Néel order observed in strongly underdoped NCCO, coexistence of antiferromagnetism and superconductivity in electron-doped cuprates remains controversial. A number of neutron scattering and muon-spin rotation studies [53–56] have detected short-range Néel fluctuations but no static order within the superconducting doping range. However, another group of neutron scattering [57, 58] and magnetotransport [59–61] experiments have produced evidence of static or quasi-static AF order in superconducting samples at least up to optimal doping  $x_{opt}$ . Alternative mechanisms of the Fermi surface reconstruction have been proposed, including a  $d$ -density wave [18], a charge-density wave [19] or coexistent topological and fluctuating short-range AF orders [20].

To shed light on the possible relevance of antiferromagnetism to the electronic ground state of superconducting NCCO, we have studied the field-orientation dependence of the SdH oscillations of the interlayer resistance in an optimally doped,  $x_{opt} = 0.15$ , NCCO crystal. In line with the previous reports, the reconstructed Fermi surface has been revealed by slow oscillations with a single frequency  $F_\alpha(\theta) = 294$  T/ $\cos\theta$ , corresponding to the small hole pocket  $\alpha$  centered at the nodal points  $(\pm\pi/2a, \pm\pi/2a)$  at the magnetic Brillouin zone boundary (see inset of Fig. 4). The  $1/\cos\theta$  dependence of the frequency confirms the quasi-2D character of the conduction.

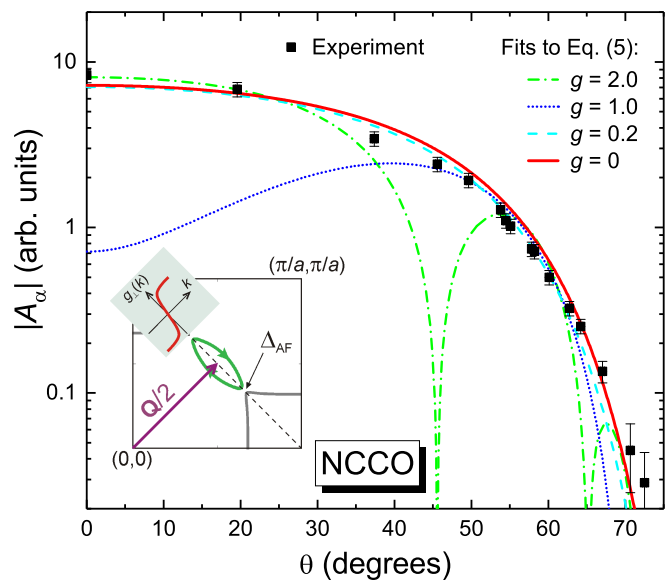


FIG. 4: Angular dependence of the SdH amplitude in optimally doped NCCO. The lines are fits to Eq. (5) with different values of the  $g$ -factor. Inset: The first quadrant of the Brillouin zone with the Fermi surface reconstructed by a superlattice potential with the wave vector  $\mathbf{Q} = (\pi/a, \pi/a)$ . If this potential involves Néel order, the function  $g_\perp(\mathbf{k})$  vanishes at the reduced Brillouin zone boundary (dashed line), as shown by the thick red line in the inset. The SdH oscillations are associated with the hole pocket (green oval) centered at  $(\pi/2a, \pi/2a)$  [14].

The main panel of Fig. 4 presents the angular dependence of the oscillation amplitude (symbols), in a field rotated in the  $(ac)$  plane (normal to the layers). The amplitude was determined by FFT of the data taken at  $T = 2.5$  K in the field window  $45 \leq B \leq 64$  T. The lines in the figure are fits to the Lifshitz-Kosevich formula (5), for different  $g$ -factors. The fits were performed using the MB factor  $R_{MB} = [1 - \exp(-B_0/B)]$  [50, 52], the reported values for the MB field  $B_0 = 12.5$  T, and the effective cyclotron mass  $m(\theta = 0^\circ) = 1.05m_0$  [52], while taking into account the  $1/\cos\theta$  angular dependence of both  $B_0$  and  $m$ . The prefactor  $A_0$  and Dingle temperature  $T_D$  were used as fit parameters, yielding  $T_D = 12.2 \pm 0.6$  K, close to the value found in the earlier experiment [52].

Similarly to  $\kappa$ -BETS, the oscillation amplitude in NCCO decreases by a factor of about 300, with no sign of spin-zeros as the field is tilted from  $\theta = 0^\circ$  to  $\theta \approx 72.5^\circ$ . Again, this behavior is in stark contrast to what one would expect for the textbook value  $g = 2$ , which would have produced two spin-zeros in the interval  $0^\circ \leq \theta \leq 70^\circ$ , see the green dash-dotted line in Fig. 4. A reduction of the  $g$ -factor to 1.0 would shift the first spin-zero to about  $72^\circ$ , near the edge of our range (blue dotted line in Fig. 4). However, this would simultaneously suppress the amplitude at small  $\theta$  by a factor of ten, contrary to our observations. All in all, our analysis

shows that a finite constant  $g$  could be compatible with the experimental data only if smaller than 0.2.

*Discussion* — In both materials, our data impose on the effective  $g$ -factor an upper bound of 0.2. At first sight, one could simply view this as a suppression of the effective  $g$  to a finite value, inferior to 0.2. However, we argue that, in fact, our findings imply  $\bar{g}_\perp = 0$  and point to the importance of the Zeeman SOC in both materials.

In the organic salt, this choice is facilitated by virtue of explaining the data based only on the interplay between the crystal symmetry and the periodicity of the Néel state [5, 6, 34]. In  $\kappa$ -BETS this interplay guarantees that  $g_\perp(\mathbf{k})$  vanishes on the entire line  $k_c = \pi/2c$  and is an odd function of  $k_c - \pi/2c$ , as shown in the inset of Fig. 1, see also SM [23]. The  $\delta$  orbit is centered on the line  $k_c = \pi/2c$ ; hence  $\bar{g}_\perp$  in Eqs. (3) and (4) vanishes, implying the absence of spin-zeros, in agreement with our data. At the same time, quantum oscillations in the paramagnetic phase clearly reveal the Zeeman splitting of Landau levels with  $g = 2.0$ . Therefore, we conclude that  $\bar{g}_\perp = 0$  is an intrinsic property of the Néel state.

In NCCO, as already mentioned, the presence of a (quasi)static Néel order at the optimal doping has been a subject of debate. However, if indeed present, such an order leads to  $g_\perp(\mathbf{k}) = 0$  at the entire magnetic Brillouin zone boundary [23]. The hole pockets, responsible for the observed  $F_\alpha \simeq 300$  T oscillations, are believed to be centered at momentum  $(\frac{\pi}{2}, \frac{\pi}{2})$ , yielding  $\bar{g}_\perp = 0$  by symmetry of  $g_\perp(\mathbf{k})$  (see [23] and the inset of Fig. 4). Such an interpretation requires that the relevant AF fluctuations have frequencies below the cyclotron frequency in our experiment,  $\nu_c \sim 10^{12}$  Hz at 50 T.

Thus, we interpret the absence of spin-zeros in the AF  $\kappa$ -BETS and in optimally doped NCCO as a manifestation of the Zeeman SOC. Our explanation relies only on the symmetry of the Néel state and the location of the carrier pockets, while being insensitive to the mechanism of the antiferromagnetism or to the orbital makeup of the relevant bands.

The work was supported by HLD at HZDR, a member of the European Magnetic Field Laboratory (EMFL). P. D. G. is supported by the Foundation for the Advancement of Theoretical Physics and Mathematics “BASIS”. R. G. acknowledges financial support from the German Research Foundation (DFG) via Germany’s Excellence Strategy (EXC-2111-390814868). J. W. acknowledges financial support from the German Research Foundation (DFG) through the Würzburg-Dresden Cluster of Excellence on Complexity and Topology in Quantum Matter - ct.qmat (EXC 2147, project-id 39085490). P. D. G. thanks the Laboratoire de Physique Théorique, Toulouse, for the hospitality during his visit.

\* revaz@irsamc.ups-tlse.fr

† grigorev@itp.ac.ru

‡ Present address: Hochfeld-Magnetlabor Dresden (HLD-EMFL), Helmholtz-Zentrum Dresden-Rossendorf, 01328 Dresden, Germany

§ TNG Technology Consulting GmbH, 85774 Unterföhring, Germany

¶ mark.kartsovnik@wmi.badw.de

- [1] R. Winkler, Spin-orbit Coupling Effects in Two-dimensional Electron and Hole Systems, Springer Tracts in Modern Physics, Vol. 191, Berlin – Heidelberg, 2003.
- [2] M. I. Dyakonov (Editor), Spin Physics in Semiconductors, Springer Series in Solid-State Sciences, Vol. 157, Berlin – Heidelberg, 2017.
- [3] V. B. Berestetskii, E. M. Lifshitz and L. P. Pitaevskii, “Course of Theoretical Physics”, Vol. 4, *Quantum Electrodynamics*, Pergamon Press (1982).
- [4] C. Kittel, Quantum Theory of Solids, John Wiley & Sons, Inc., New York – London, 1963.
- [5] R. Ramazashvili, Phys. Rev. Lett. **101**, 137202 (2008).
- [6] R. Ramazashvili, Phys. Rev. B **79**, 184432 (2009).
- [7] S. A. Brazovskii and I. A. Luk’yanchuk, Sov. Phys. JETP **69**, 1180 (1989).
- [8] S. A. Brazovskii, I. A. Luk’yanchuk, and R. R. Ramazashvili, JETP Lett. **49**, 644 (1989).
- [9] V.V. Kabanov and A. S. Alexandrov, Phys. Rev. B **77**, 132403 (2008); **81**, 099907(E) (2010).
- [10] R. Ramazashvili, Phys. Rev. B **80**, 054405 (2009).
- [11] H. Fujiwara, E. Fujiwara, Y. Nakazawa, B. Zh. Narymbetov, K. Kato, H. Kobayashi, A. Kobayashi, M. Tokumoto, and P. Cassoux, J. Am. Chem. Soc. **123**, 306 (2001).
- [12] N. P. Armitage, P. Fournier, and R. L. Greene, Rev. Mod. Phys. **82**, 2421 (2010).
- [13] D. Shoenberg, Magnetic Oscillations in Metals (Cambridge University Press, 1984).
- [14] T. Helm, M. V. Kartsovnik, M. Bartkowiak, N. Bittner, M. Lambacher, A. Erb, J. Wosnitza, and R. Gross, Phys. Rev. Lett. **103**, 157002 (2009).
- [15] T. Konoike, S. Uji, T. Terashima, M. Nishimura, S. Yasuzuka, K. Enomoto, H. Fujiwara, E. Fujiwara, B. Zhang, and H. Kobayashi, Phys. Rev. B **72**, 094517 (2005).
- [16] T. Das, R. S. Markiewicz, and A. Bansil, J. Phys. Chem. Solids **69**, 2963 (2008).
- [17] S. Sachdev, Phys. Status Solidi B **247**, 537 (2010).
- [18] S. Chakravarty, R. B. Laughlin, D. K. Morr, and C. Nayak, Phys. Rev. B **63**, 094503 (2001).
- [19] E. H. da Silva Neto, R. Comin, F. He, R. Sutarto, Y. Jiang, R. L. Greene, G. A. Sawatzky, and A. Damascelli, Science **347**, 282 (2015).
- [20] S. Sachdev, Rep. Prog. Phys. **82**, 014001 (2019); S. Sachdev, H. D. Scammell, M. S. Scheurer, and G. Tarnopolsky, Phys. Rev. B **99**, 054516 (2019).
- [21] S. E. Sebastian, N. Harrison, C. H. Mielke, Ruixing Liang, D. A. Bonn, W. N. Hardy, and G. G. Lonzarich, Phys. Rev. Lett. **103**, 256405 (2009).
- [22] B. J. Ramshaw, B. Vignolle, J. Day, R. Liang, W. N. Hardy, C. Proust, and D. A. Bonn, Nature Physics **7**, 234 (2011).
- [23] See Supplemental Material at [URL to be provided by the publisher] for the derivation of the Fermi surface splitting

- in the presence of Zeeman spin-orbit coupling, the symmetry analysis of the Néel state in  $\kappa$ -BETS and in NCCO, an estimate of  $k_F\xi$  in these two materials, the symmetry properties of  $g_{\perp}(\mathbf{k})$ , and discussion of the fit quality for  $\kappa$ -BETS. The Supplemental Material also includes Refs. [24–28].
- [24] N. I. Kulikov and V. V. Tugushev, *Usp. Fiz. Nauk* **144**, 643 (1984) [*Sov. Phys. Usp.* **27**, 954 (1984)].
- [25] L. M. Falicov and H. Stachowiak, *Phys. Rev.* **147**, 505 (1966).
- [26] J. Wosnitza, *Fermi Surfaces of Low-Dimensional Organic Metals and Superconductors*, Springer Verlag, Berlin – Heidelberg, 1996.
- [27] M. V. Kartsovnik, *Chem. Rev.* **104**, 5737 (2004).
- [28] E. I. Blount, *Phys. Rev.* **126**, 1636 (1962).
- [29] J. Wosnitza, G. W. Crabtree, H. H. Wang, U. Geiser, J. M. Williams, and K. D. Carlson, *Phys. Rev. B*, **45**, 3018 (1992).
- [30] A. E. Kovalev, M. V. Kartsovnik, and N. D. Kushch, *Solid State Commun.* **87**, 705 (1993).
- [31] F. A. Meyer, E. Steep, W. Biberacher, P. Christ, A. Lerf, A. G. M. Jansen, W. Joss, P. Wyder, and K. Andres, *Europhys. Lett.* **32**, 681 (1995).
- [32] S. Uji, C. Terakura, T. Terashima, T. Yakabe, Y. Terai, M. Tokumoto, A. Kobayashi, F. Sakai, H. Tanaka, and H. Kobayashi, *Phys. Rev. B* **65**, 113101 (2002).
- [33] M. V. Kartsovnik, M. Kunz, L. Schaidhammer, F. Kollmannsberger, W. Biberacher, N.D. Kushch, A. Miyazaki, and H. Fujiwara, *J. Supercond. Nov. Magn.* **29**, 3075 (2016).
- [34] R. Ramazashvili, *Phys. Rev. Lett.* **105**, 216404 (2010).
- [35] M. R. Norman and J. Lin, *Phys. Rev. B* **82**, 060509(R) (2010).
- [36] S. Uji, H. Shinagawa, Y. Terai, T. Yakabe, C. Terakura, T. Terashima, L. Balicas, J. S. Brooks, E. Ojima, H. Fujiwara, H. Kobayashi, A. Kobayashi, and M. Tokumoto, *Physica B* **298**, 557 (2001).
- [37] T. Mori and M. Katsuhara, *J. Phys. Soc. Jpn.* **71**, 826 (2002).
- [38] T. Konoike, S. Uji, T. Terashima, M. Nishimura, S. Yasuzuka, K. Enomoto, H. Fujiwara, B. Zhang, and H. Kobayashi, *Phys. Rev. B* **70**, 094514 (2004).
- [39] O. Cépas, R. H. McKenzie, and J. Merino, *Phys. Rev. B* **65**, 100502(R) (2002).
- [40] R. E. Peierls, *Quantum Theory of Solids* (Oxford University Press, 2001).
- [41] T. Konoike, S. Uji, T. Terashima, M. Nishimura, T. Yamaguchi, K. Enomoto, H. Fujiwara, B. Zhang, and H. Kobayashi, *J. Low Temp. Phys.* **142**, 531 (2006).
- [42] S. Massidda, N. Hamada, J. Yu, and A. J. Freeman, *Physica C* **157**, 571 (1989).
- [43] O. K. Andersen, A. I. Liechtenstein, O. Jepsen, and F. Paulsen, *J. Phys. Chem. Solids* **56**, 1573 (1995).
- [44] N. P. Armitage, F. Ronning, D. H. Lu, C. Kim, A. Damascelli, K. M. Shen, D. L. Feng, H. Eisaki, Z.-X. Shen, P. K. Mang, N. Kaneko, M. Greven, Y. Onose, Y. Taguchi, and Y. Tokura, *Phys. Rev. Lett.* **88**, 257001 (2002).
- [45] H. Matsui, T. Takahashi, T. Sato, K. Terashima, H. Ding, T. Uefuji, and K. Yamada, *Phys. Rev. B* **75**, 224514 (2007).
- [46] A. F. Santander-Syro, M. Ikeda, T. Yoshida, A. Fujimori, K. Ishizaka, M. Okawa, S. Shin, R. L. Greene, and N. Bontemps, *Phys. Rev. Lett.* **106**, 197002 (2011).
- [47] D. Song, G. Han, W. Kyung, J. Seo, S. Cho, B-S. Kim, M. Arita, K. Shimada, H. Namatame, M. Taniguchi, Y. Yoshida, H. Eisaki, S-R. Park, and C. Kim, *Phys. Rev. Lett.* **118**, 137001 (2017).
- [48] J.-F. He, C. R. Rotundu, M. S. Scheurer, Y. He, M. Hashimoto, K. Xu, Y. Wang, E. W. Huang, T. Jia, S.-D. Chen, B. Moritz, D.-H. Lu, Y. S. Lee, T. P. Devereaux, and Z.-X. Shen, *Proc. Natl. Acad. Sci. USA* **116**, 3449 (2019).
- [49] T. Helm, M. V. Kartsovnik, I. Sheikin, M. Bartkowiak, F. Wolff-Fabris, N. Bittner, W. Biberacher, M. Lambacher, A. Erb, J. Wosnitza, and R. Gross, *Phys. Rev. Lett.* **105**, 247002 (2010).
- [50] M. V. Kartsovnik, T. Helm, C. Putzke, F. Wolff-Fabris, I. Sheikin, S. Lepault, C. Proust, D. Vignolles, N. Bittner, W. Biberacher, A. Erb, J. Wosnitza, and R. Gross, *New J. Phys.* **13**, 015001 (2011).
- [51] J. S. Higgins, M. K. Chan, T. Sarkar, R. D. McDonald, R. L. Greene, and N. P. Butch, *New Journal of Physics* **20**, 043019 (2018).
- [52] T. Helm, M. V. Kartsovnik, C. Proust, B. Vignolle, C. Putzke, E. Kampert, I. Sheikin, E.-S. Choi, J. S. Brooks, N. Bittner, W. Biberacher, A. Erb, J. Wosnitza, and R. Gross, *Phys. Rev. B* **92**, 094501 (2015).
- [53] G. M. Luke, L. P. Le, B. J. Sternlieb, Y. J. Uemura, J. H. Brewer, R. Kadono, R. F. Kiefl, S. R. Kreitzman, T. M. Riseman, C. E. Stronach, M. R. Davis, S. Uchida, H. Takagi, Y. Tokura, Y. Hidaka, T. Murakami, J. Gopalakrishnan, A. W. Sleight, M. A. Subramanian, E. A. Early, J. T. Markert, M. B. Maple, and C. L. Seaman, *Phys. Rev. B* **42**, 7981 (1990).
- [54] E. M. Motoyama, G. Yu, I. M. Vishik, O. P. Vajk, P. K. Mang, and M. Greven, *Nature* **445**, 186 (2007).
- [55] P. K. Mang, S. Larochelle, A. Mehta, O. P. Vajk, A. S. Erickson, L. Lu, W. J. L. Buyers, A. F. Marshall, K. Prokes, and M. Greven, *Phys. Rev. B* **70**, 094507 (2004).
- [56] H. Saadaoui, Z. Salman, H. Luetkens, T. Prokscha, A. Suter, W. A. MacFarlane, Y. Jiang, K. Jin, R. L. Greene, E. Morenzoni, and R. F. Kiefl, *Nat. Comm.* **6**, 6041 (2015).
- [57] K. Yamada, K. Kurahashi, T. Uefuji, M. Fujita, S. Park, S.-H. Lee, and Y. Endoh, *Phys. Rev. Lett.* **90**, 137004 (2003).
- [58] H. J. Kang, P. Dai, H. A. Mook, D. N. Argyriou, V. Sikolenko, J. W. Lynn, Y. Kurita, S. Komiya, and Y. Ando, *Phys. Rev. B* **71**, 214512 (2005).
- [59] Y. Dagan, M. C. Barr, W. M. Fisher, R. Beck, T. Dhakal, A. Biswas, and R. L. Greene *Phys. Rev. Lett.* **94**, 057005 (2005).
- [60] W. Yu, J. S. Higgins, P. Bach, and R. L. Greene *Phys. Rev. B* **76**, 020503(R) (2007).
- [61] A. Dorantes, A. Alshemi, Z. Huang, A. Erb, T. Helm, and M. V. Kartsovnik, *Phys. Rev. B* **97**, 054430 (2018).

# Supplemental Material to “Zeeman spin-orbit coupling and magnetic quantum oscillations in antiferromagnetic conductors”

R. Ramazashvili,<sup>1,\*</sup> P. D. Grigoriev,<sup>2,3,4,†</sup> T. Helm,<sup>5,6,‡</sup> F. Kollmannsberger,<sup>5,6</sup>  
 M. Kunz,<sup>5,6,§</sup> W. Biberacher,<sup>5</sup> E. Kampert,<sup>7</sup> H. Fujiwara,<sup>8</sup> A.  
 Erb,<sup>5,6</sup> J. Wosnitza,<sup>7,9</sup> R. Gross,<sup>5,6,10</sup> and M. V. Kartsovnik<sup>5,¶</sup>

<sup>1</sup>*Laboratoire de Physique Théorique,  
 Université de Toulouse, CNRS, UPS, France*

<sup>2</sup>*L. D. Landau Institute for Theoretical Physics, 142432 Chernogolovka, Russia*

<sup>3</sup>*National University of Science and Technology MISiS, 119049 Moscow, Russia*

<sup>4</sup>*P.N. Lebedev Physical Institute, 119991 Moscow, Russia*

<sup>5</sup>*Walther-Meißner-Institut, Bayerische Akademie der Wissenschaften,  
 Walther-Meißner-Strasse 8, D-85748 Garching, Germany*

<sup>6</sup>*Physik-Department, Technische Universität München, D-85748 Garching, Germany*

<sup>7</sup>*Hochfeld-Magnetlabor Dresden (HLD-EMFL) and  
 Würzburg-Dresden Cluster of Excellence ct.qmat,  
 Helmholtz-Zentrum Dresden-Rossendorf, 01328 Dresden, Germany*

<sup>8</sup>*Department of Chemistry, Graduate School of Science,  
 Osaka Prefecture University, Osaka 599-8531, Japan*

<sup>9</sup>*Institut für Festkörper- und Materialphysik,  
 TU Dresden, 01062 Dresden, Germany*

<sup>10</sup>*Munich Center for Quantum Science and  
 Technology (MCQST), D-80799 Munich, Germany*

(Dated: today)

---

\* revaz@irsamc.ups-tlse.fr

† grigorev@itp.ac.ru

‡ Present address: Hochfeld-Magnetlabor Dresden (HLD-EMFL), Helmholtz-Zentrum Dresden-Rossendorf,  
01328 Dresden, Germany

§ TNG Technology Consulting GmbH, 85774 Unterföhring, Germany

¶ mark.kartsovnik@wmi.badw.de

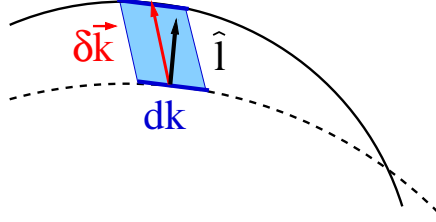


FIG. S1. Fermi surface of a two-dimensional conductor in zero field (dashed line) and in a transverse field  $\mathbf{B}_\perp$  (solid line). Upon turning on the  $\mathbf{B}_\perp$ , a Fermi surface element  $dk$  shifts by a small momentum  $\delta\mathbf{k}$  (see the main text), adding the shaded trapezoid of the area  $d\mathcal{F} = dk(\delta\mathbf{k} \cdot \hat{\mathbf{l}}_{\mathbf{k}})$  to the area enclosed by the Fermi surface, where  $\hat{\mathbf{l}}_{\mathbf{k}} = \nabla_{\mathbf{k}}\mathcal{E}(\mathbf{k})/|\nabla_{\mathbf{k}}\mathcal{E}(\mathbf{k})|$  is the local unit vector, normal to the Fermi surface. The total variation of the Fermi area is given by integrating the  $d\mathcal{F}$  over the Fermi surface, as explained in the main text.

### A. SPIN REDUCTION FACTOR $R_s(\theta)$ IN A MAGNETIC FIELD PERPENDICULAR TO THE NÉEL AXIS

As pointed out in the main text, in a purely transverse field  $\mathbf{B}_\perp$  the single-particle Hamiltonian takes the form  $\mathcal{H} = \mathcal{E}(\mathbf{k}) - \frac{1}{2}\mu_B g_\perp(\mathbf{k})(\mathbf{B}_\perp \cdot \boldsymbol{\sigma})$ , where  $\mathcal{E}(\mathbf{k})$  is the zero-field dispersion near the Fermi surface, and  $\boldsymbol{\sigma} = (\sigma^x, \sigma^y, \sigma^z)$  is the vector, made of the three Pauli spin matrices. Upon turning on the field, a given point  $\mathbf{k}$  of the Fermi surface undergoes a small shift  $\delta\mathbf{k}$  such that  $\delta\mathbf{k} \cdot \nabla_{\mathbf{k}}\mathcal{E}(\mathbf{k}) = \pm\frac{1}{2}\mu_B g_\perp(\mathbf{k})B_\perp$ , where the  $\pm$  signs correspond to the ‘up’ and ‘down’ spin projections on  $\mathbf{B}_\perp$  and to the subscript of the resulting Fermi surface areas  $\mathcal{F}_\pm$ . As shown in Fig. S1, upon the shift by  $\delta\mathbf{k}$  an element  $dk$  of the Fermi surface contributes the shaded area  $dk(\delta\mathbf{k} \cdot \hat{\mathbf{l}}_{\mathbf{k}}) = \pm\frac{1}{2}\mu_B H_\perp dk g_\perp(\mathbf{k})/|\nabla_{\mathbf{k}}\mathcal{E}(\mathbf{k})|$  to the variation of the total area, enclosed by the Fermi surface. Here  $\hat{\mathbf{l}}_{\mathbf{k}} = \nabla_{\mathbf{k}}\mathcal{E}(\mathbf{k})/|\nabla_{\mathbf{k}}\mathcal{E}(\mathbf{k})|$  is the local unit vector, normal to the Fermi surface. Therefore, to linear order in  $B_\perp$ , the areas  $\mathcal{F}_\pm$  of the two spin-split Fermi surfaces differ by

$$\delta\mathcal{F} = \mathcal{F}_+ - \mathcal{F}_- = \mu_B H_\perp \oint_{FS} \frac{dk g_\perp(\mathbf{k})}{|\nabla_{\mathbf{k}}\mathcal{E}(\mathbf{k})|}, \quad (\text{S1})$$

where the line integral is taken along the zero-field Fermi surface. Combined, Eqs. (3) and (S1) yield Eq. (4).

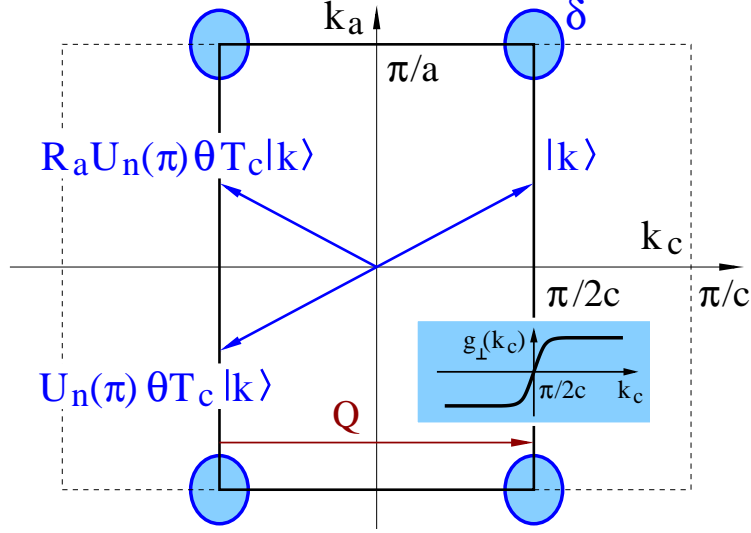


FIG. S2. Schematic view of the Brillouin zone of  $\kappa$ -BETS in its paramagnetic state (dashed line) and in the Néel state (solid line). The  $\delta$  pocket is centered at the corner  $\mathbf{k} = (\pm\pi/2c, \pm\pi/a)$  of the magnetic Brillouin zone. The arrows show an exact Bloch eigenstate  $|\mathbf{k}\rangle$  at a wave vector  $\mathbf{k}$  on the vertical segment  $k_c = \pi/2c$  of the magnetic Brillouin zone boundary – and its symmetry partners  $\theta\mathbf{T}_c\mathbf{U}_n(\pi)|\mathbf{k}\rangle$  and  $\theta\mathbf{T}_c\mathbf{R}_a\mathbf{U}_n(\pi)|\mathbf{k}\rangle$ . The orthogonality  $\langle\mathbf{k}|\mathbf{R}_a\mathbf{U}_n(\pi)\theta\mathbf{T}_c|\mathbf{k}\rangle = 0$  implies that  $g_\perp(\mathbf{k})$  vanishes on the segment  $k_c = \pi/2c$ . The inset illustrates the  $g_\perp(\mathbf{k})$  being an odd function of  $k_c - \pi/2c$ .

## B. SYMMETRY ANALYSIS OF THE NÉEL STATE OF $\kappa$ -(BETS)<sub>2</sub>FeBr<sub>4</sub> IN A TRANSVERSE FIELD

The existence of a special set of momenta in the Brillouin zone, where Bloch eigenstates of a Néel antiferromagnet remain degenerate in transverse magnetic field, is a general phenomenon. However, the precise geometry of this set depends on the interplay between the periodicity of the Néel order and the symmetry of the underlying crystal lattice [S1, S2]. Here we describe this set for  $\kappa$ -(BETS)<sub>2</sub>FeBr<sub>4</sub>, hereafter referred to as  $\kappa$ -BETS.

Upon transition from the paramagnetic to Néel state, the lattice period of  $\kappa$ -BETS along the  $c$  axis doubles, and the symmetry of the paramagnetic state with respect to both the time reversal  $\hat{\theta}$  and the elementary translation  $\hat{\mathbf{T}}_c$  along the  $c$  axis is broken. Yet the product  $\hat{\theta}\hat{\mathbf{T}}_c$  remains a symmetry operation, along with spin rotation  $\hat{\mathbf{U}}_{\mathbf{n}}(\phi)$  around the Néel axis  $\mathbf{n}$  by an arbitrary angle  $\phi$ .

Applied transversely to  $\mathbf{n}$ , a magnetic field breaks the symmetry with respect to both  $\hat{\theta}\hat{\mathbf{T}}_c$  and  $\hat{\mathbf{U}}_{\mathbf{n}}(\phi)$ ; however,  $\hat{\mathbf{U}}_{\mathbf{n}}(\pi)\hat{\theta}\hat{\mathbf{T}}_c$  remains a symmetry operation [S1, S2]. It maps a Bloch eigenstate  $|\mathbf{k}\rangle$  at wave vector  $\mathbf{k}$  onto a degenerate orthogonal eigenstate  $\hat{\mathbf{U}}_{\mathbf{n}}(\pi)\hat{\theta}\hat{\mathbf{T}}_c|\mathbf{k}\rangle$  at wave vector  $-\mathbf{k}$ , as shown in Fig. S2. Upon combination with reflection  $\hat{\mathbf{R}}_a: (k_c, k_a) \rightarrow (k_c, -k_a)$ , the resulting symmetry operation  $\hat{\mathbf{R}}_a\hat{\mathbf{U}}_{\mathbf{n}}(\pi)\hat{\theta}\hat{\mathbf{T}}_c$  maps  $|\mathbf{k}\rangle$  at wave vector  $\mathbf{k} = (k_c, k_a)$  onto a degenerate orthogonal eigenstate  $\hat{\mathbf{R}}_a\hat{\mathbf{U}}_{\mathbf{n}}(\pi)\hat{\theta}\hat{\mathbf{T}}_c|\mathbf{k}\rangle$  at wave vector  $(-k_c, k_a)$  [S1, S2].

For an arbitrary  $\mathbf{k} = (k_c, k_a)$  at the vertical segment  $k_c = \pi/2c$  of the magnetic Brillouin zone boundary, the wave vectors  $(-k_c, k_a)$  and  $(k_c, k_a)$  differ by the reciprocal wave vector  $\mathbf{Q} = (\pi/c, 0)$  of the Néel state; in the nomenclature of the magnetic Brillouin zone, they are one and the same vector. The degeneracy of such a  $|\mathbf{k}\rangle$  with  $\hat{\theta}\hat{\mathbf{T}}_c\hat{\mathbf{R}}_a\hat{\mathbf{U}}_{\mathbf{n}}(\pi)|\mathbf{k}\rangle$  means that  $g_{\perp}(\mathbf{k})$  vanishes at the entire segment  $k_c = \pi/2c$ .

The  $\delta$  pocket is centered at  $(\pm\pi/2c, \pm\pi/a)$  and is symmetric with respect to reflection around the line  $k_c = \pm\pi/2c$ , as shown in Figs. 1 and S2. At the same time, as shown in Supplemental Material E and illustrated in the insets of Figs. 1 and S2,  $g_{\perp}(\mathbf{k})$  is odd under reflection around the same line. As a result, for the  $\delta$  pocket  $\bar{g}_{\perp}$  in Eq. (5) vanishes, as stated in the main text.

### C. SYMMETRY ANALYSIS OF THE NÉEL STATE OF $\text{Nd}_{2-x}\text{Ce}_x\text{CuO}_4$ IN A TRANSVERSE FIELD

In the antiferromagnetic state of  $\text{Nd}_{2-x}\text{Ce}_x\text{CuO}_4$  (hereafter NCCO), the  $\text{Cu}^{2+}$  spins point along the layers. At zero field, they form a so-called non-collinear structure: the staggered magnetization vectors of adjacent layers are normal to each other, pointing along the crystallographic directions [100] and [010], respectively (see Ref. [S3] for a review). However, an in-plane field above 5 T transforms this spin structure into a collinear one, with the staggered magnetization in all the layers aligned transversely to the field. Therefore, in our experiment, with the field  $B > 45$  T rotated around the [100] axis, the staggered magnetization is normal to the field at all tilt angles except for a narrow interval  $0^\circ < |\theta| \lesssim 5^\circ$ .

Thus, we can restrict ourselves to the purely transverse field geometry, with the field normal to the Néel axis, which makes the analysis similar to that for  $\kappa$ -BETS. The only difference is that, given the tetragonal symmetry of NCCO, the triple product  $\hat{\mathbf{U}}_{\mathbf{n}}(\pi)\hat{\theta}\hat{\mathbf{T}}_a$  can now be combined with reflections  $\hat{\mathbf{R}}_x: (k_x, k_y) \rightarrow (-k_x, k_y)$  and  $\hat{\mathbf{R}}_y: (k_x, k_y) \rightarrow (k_x, -k_y)$ .

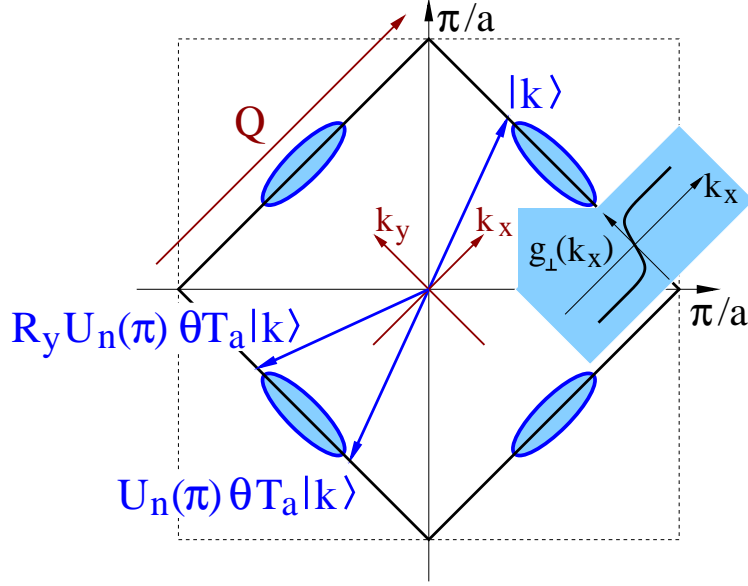


FIG. S3. Schematic view of the Brillouin zone of NCCO in its paramagnetic state (dashed line) and in the Néel state (solid line). The carrier pockets  $\alpha$  are centered at the midpoints  $\mathbf{k} = (\pm\pi/2a, \pm\pi/2a)$  of the magnetic Brillouin zone boundary. The blue arrows show an exact Bloch eigenstate  $|\mathbf{k}\rangle$  at a wave vector  $\mathbf{k}$  on the magnetic Brillouin zone boundary – and its symmetry partners  $\mathbf{U}_n(\pi)\theta\mathbf{T}_a|\mathbf{k}\rangle$  and  $\mathbf{R}_y\mathbf{U}_n(\pi)\theta\mathbf{T}_a|\mathbf{k}\rangle$ . The orthogonality  $\langle\mathbf{k}|\mathbf{R}_y\mathbf{U}_n(\pi)\theta\mathbf{T}_a|\mathbf{k}\rangle = 0$  implies that  $g_\perp(\mathbf{k})$  vanishes on the segment  $k_x a = \pm\pi/\sqrt{2}$ . The inset illustrates the  $g_\perp(\mathbf{k})$  being an odd function of  $k_x a - \pi/\sqrt{2}$ .

As a result, for any wave vector  $\mathbf{k}$  at the magnetic Brillouin zone boundary, one finds  $\langle\mathbf{k}|\hat{\mathbf{R}}_y\hat{\mathbf{U}}_n(\pi)\hat{\theta}\hat{\mathbf{T}}_a|\mathbf{k}\rangle = \langle\mathbf{k}|\hat{\mathbf{R}}_x\hat{\mathbf{U}}_n(\pi)\hat{\theta}\hat{\mathbf{T}}_a|\mathbf{k}\rangle = 0$ . This guarantees double degeneracy of Bloch eigenstates, hence the equality  $g_\perp(\mathbf{k}) = 0$  at the entire boundary of the magnetic Brillouin zone, as shown in Fig. S3.

The charge carrier pockets of our interest are believed to be centered at  $(\pm\pi/2a, \pm\pi/2a)$ , and are symmetric with respect to reflections  $\mathbf{R}_x$  and  $\mathbf{R}_y$  around the  $k_x$  and  $k_y$  axes, as shown in Figs. 4 and S3. At the same time, as shown in Section E and illustrated in the inset of Figs. 4 and S3,  $g_\perp(\mathbf{k})$  is odd under the very same reflections. As a result,  $\bar{g}_\perp$  in Eq. (5) vanishes for these pockets, as stated in the main text.

## D. ESTIMATING THE PRODUCT $k_F\xi$

### 1. $\delta$ pocket in $\kappa$ -BETS:

Looking only for a crude estimate, we assume a parabolic energy dispersion and treat the  $\delta$  pocket as circular, of radius  $k_F$  and area  $\mathcal{F}_\delta = 2\pi eF_\delta/\hbar$ . Defining the antiferromagnetic coherence length as  $\xi = \hbar v_F/\Delta_{\text{AF}}$ , we find:

$$k_F\xi = \hbar k_F v_F/\Delta_{\text{AF}} = 2\varepsilon_F/\Delta_{\text{AF}}. \quad (\text{S2})$$

The Fermi energy  $\varepsilon_F$  in Eq. (S2) can be expressed via the Shubnikov-de Haas (SdH) frequency  $F_\delta = 61$  T:

$$\varepsilon_F = \frac{\hbar^2 k_F^2}{2m} = \frac{\hbar^2 \mathcal{F}_\delta}{2\pi m} = \frac{\hbar e F_\delta}{m} \approx 6 \text{ meV}. \quad (\text{S3})$$

Assuming a BSC-like relation between the Néel temperature,  $T_N \approx 2.5$  K, and the antiferromagnetic gap  $\Delta_{\text{AF}}$  in the electron spectrum, we evaluate the latter as  $\Delta_{\text{AF}} \simeq 1.8k_B T_N \approx 0.4$  meV. A similar estimate is obtained from the critical field,  $B_c \approx 5$  T, required to suppress the Néel state:  $\Delta_{\text{AF}} \sim \mu_B B_c \approx 0.3$  meV.

Thus we find  $k_F\xi \simeq \frac{2\varepsilon_F}{\Delta_{\text{AF}}} \sim 30 - 40 \gg 1$ , which means that  $g_\perp(\mathbf{k})$  is nearly constant over most of the Fermi surface, except a small vicinity of  $k_c = \pi/2c$ , where it changes sign, cf. Figs. S2 and S4.

### 2. Small hole pocket of the reconstructed Fermi surface in NCCO:

In NCCO, the small Fermi pocket  $\alpha$ , responsible for the observed oscillations, is far from being circular. Therefore, we can no longer estimate  $k_F\xi$  the same way as we did for the  $\delta$  pocket in  $\kappa$ -BETS. Instead, we evaluate the relevant Fermi wave vector and the antiferromagnetic coherence length separately.

The value of the Fermi wave vector in the direction normal to the magnetic Brillouin zone boundary can be found from ARPES maps of the Fermi surface [S5–S7]:  $k_F = 0.4 \pm 0.1 \text{ nm}^{-1}$ .

The coherence length can be estimated using the MB gap value,  $\Delta_{\text{AF}} \approx 16$  meV, and parameters of the (approximately circular) large parent Fermi surface obtained from the analysis of MB quantum oscillations [S4]. Using the corresponding SdH frequency  $F = 11.25$  kT and cyclotron mass  $m_c = 3.0m_e$ , we estimate the Fermi velocity,  $v_F \sim \hbar k_F/m_c \approx \sqrt{2\hbar e F}/m_c \approx 2.2 \times 10^5$  m/s, which leads to the coherence length  $\xi \sim \hbar v_F/\Delta_{\text{AF}} \approx 9$  nm.

This yields the product  $k_F\xi \sim 3 - 5$ , which implies  $g_\perp(\mathbf{k})$  being piecewise nearly constant over most of the Fermi surface, except a small vicinity of the magnetic Brillouin zone boundary, where  $g_\perp(\mathbf{k})$  changes sign, cf. Figs. S3 and S4.

### E. SYMMETRY PROPERTIES OF $g_\perp(\mathbf{k})$

In Section B, we have shown that in  $\kappa$ -BETS the factor  $g_\perp(\mathbf{k})$  vanishes at the entire  $k_c = \pm\pi/2c$  segment of the magnetic Brillouin zone boundary. In the present section, we establish an important general symmetry property of  $g_\perp(\mathbf{k})$ . In the case of  $\kappa$ -BETS, this property implies that  $g_\perp(\mathbf{k})$  is an odd function of  $k_c - \pi/2c$ . The  $\delta$  pocket, responsible for the observed SdH oscillations, is centered on this segment, at the corner of the magnetic Brillouin zone (see Fig. 1). As a result, for this pocket the “effective  $g$ -factor”  $\bar{g}_\perp$  in Eq. (4) vanishes by symmetry.

Without loss of generality, we consider the simplest case of double commensurability, relevant to both materials of our interest. In both of them, the underlying non-magnetic state is centrosymmetric, with the relevant electron band having the spectrum  $\varepsilon(\mathbf{k})$ . Spontaneous Néel magnetization with wave vector  $\mathbf{Q}$  interacts with the conduction electron spin  $\boldsymbol{\sigma}$  via the exchange term  $(\boldsymbol{\Delta}_{\text{AF}} \cdot \boldsymbol{\sigma})$ , coupling the states at wave vectors  $\mathbf{k}$  and  $\mathbf{k} + \mathbf{Q}$ . In the Néel phase, subjected to magnetic field  $\mathbf{B}$ , the electron Hamiltonian takes the form [S8]

$$\mathcal{H}_{\mathbf{k}} = \begin{bmatrix} \varepsilon(\mathbf{k}) - g(\mathbf{B} \cdot \boldsymbol{\sigma}) & (\boldsymbol{\Delta}_{\text{AF}} \cdot \boldsymbol{\sigma}) \\ (\boldsymbol{\Delta}_{\text{AF}} \cdot \boldsymbol{\sigma}) & \varepsilon(\mathbf{k} + \mathbf{Q}) - g(\mathbf{B} \cdot \boldsymbol{\sigma}) \end{bmatrix}, \quad (\text{S4})$$

where the factor  $\mu_B/2$  has been absorbed into the definition of  $\mathbf{B}$ , and  $\boldsymbol{\Delta}_{\text{AF}} = J\mathbf{S}$  is the product of the antiferromagnetically ordered moment  $\mathbf{S}$  and its exchange coupling  $J$  to the conduction electrons. In a purely transverse field  $\mathbf{B}_\perp \perp \boldsymbol{\Delta}_{\text{AF}}$ , the Hamiltonian (S4) can be easily diagonalized [S2, S9] to yield the spectrum

$$\mathcal{E}(\mathbf{p}) = \varepsilon_+(\mathbf{k}) \pm \sqrt{\Delta_{\text{AF}}^2 + [\varepsilon_-(\mathbf{k}) - g(\mathbf{B}_\perp \cdot \boldsymbol{\sigma})]^2}, \quad (\text{S5})$$

where  $\varepsilon_\pm(\mathbf{k}) = \frac{1}{2}[\varepsilon(\mathbf{k}) \pm \varepsilon(\mathbf{k} + \mathbf{Q})]$ . Equation (S5) shows that  $\Delta_{\text{AF}}$  is the energy gap in the electron spectrum of the Néel state. From Eq. (S5), one easily finds the effective transverse  $g$ -factor  $g_\perp(\mathbf{k})$  [S2, S10]

$$g_\perp(\mathbf{k}) = \frac{g\varepsilon_-(\mathbf{k})}{\sqrt{\Delta_{\text{AF}}^2 + \varepsilon_-^2(\mathbf{k})}}, \quad (\text{S6})$$

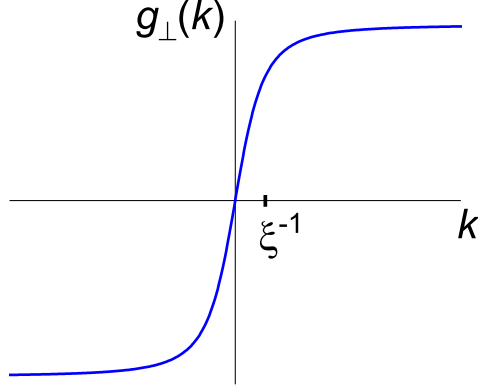


FIG. S4. Schematic plot of  $g_{\perp}(k)$  as a function of the momentum component  $k$ , normal to the line  $g_{\perp}(\mathbf{k}) = 0$ . At small  $k < 1/\xi$ , the function  $g_{\perp}(k)$  is linear:  $g_{\perp}(k) \approx g\xi k$ . Beyond  $k \approx 1/\xi$ ,  $g_{\perp}(k)$  is nearly constant:  $g_{\perp}(k) \approx g$ . Here,  $\xi = \hbar v_F/\Delta_{\text{AF}}$  is the antiferromagnetic coherence length, and  $\Delta_{\text{AF}}$  is the energy gap in the electron spectrum (S5) of the Néel state.

plotted in Fig. S4 as a function of momentum component  $k$ , normal to the line  $g_{\perp}(\mathbf{k}) = 0$ .

The parent paramagnetic state is invariant under time reversal, thus  $\varepsilon(\mathbf{k}) = \varepsilon(-\mathbf{k})$ . Also, in a doubly-commensurate antiferromagnet with Néel wave vector  $\mathbf{Q}$ , the wave vector  $2\mathbf{Q}$  is a reciprocal lattice vector of the underlying non-magnetic state; thus,  $\varepsilon(\mathbf{k} + 2\mathbf{Q}) = \varepsilon(\mathbf{k})$ . From these properties, it follows that  $\mathcal{E}(\mathbf{k}) = \mathcal{E}(-\mathbf{k} + \mathbf{Q})$  and  $g_{\perp}(\mathbf{k}) = -g_{\perp}(-\mathbf{k} + \mathbf{Q})$ . In NCCO as well as in the Néel state of  $\kappa$ -BETS, the relevant Fermi surface consists of two symmetric parts, which map onto each other under transformation  $\mathbf{k} \rightarrow -\mathbf{k} + \mathbf{Q}$ . Contributions of these two parts to the integral in the right-hand side of Eq. (S1) cancel each other exactly, hence Eq. (5) yields  $\bar{g}_{\perp} = 0$ . In other words, in Eq. (3)  $\delta\mathcal{F} = 0$ , and thus in Eqs. (3) and (4) one finds  $R_s(\theta) = 1$ : in a transverse field, the amplitude of magnetic quantum oscillations has no spin-zeros.

The arguments above rely on a quasi-classical description. Note that the key conclusion, the absence of spin-zeros in a transverse field, holds regardless of how the Fermi wave vector  $k_F$  compares with the inverse antiferromagnetic coherence length  $1/\xi \sim \Delta_{\text{AF}}/\hbar v_F$ , where the behavior of  $g_{\perp}(\mathbf{k})$  crosses over from linear to constant as illustrated in Fig. S4.

In the limit of  $k_F\xi \lesssim 1$ , the problem can be analyzed by reducing the Hamiltonian to the leading terms of its momentum expansion around the band extremum. The conclusion remains intact: in a purely transverse field, the Zeeman term of Eq. (2) does *not* lift the

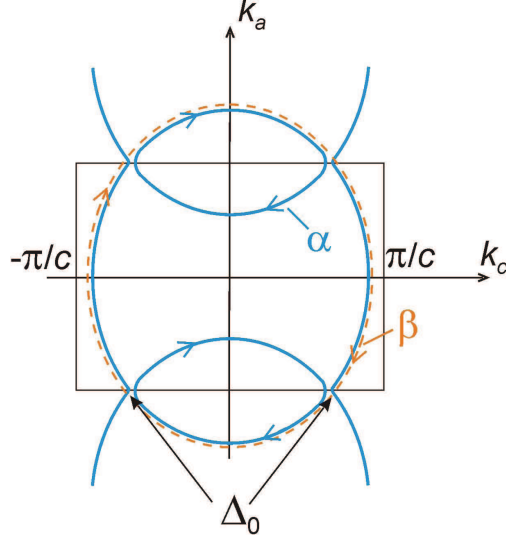


FIG. S5. Fermi surface of  $\kappa$ -BETS in the paramagnetic state [S12, S13] (blue lines). The blue arrows show the classical cyclotron orbits  $\alpha$  and the orange arrows the large MB orbit  $\beta$ , which involves tunneling through four MB gaps  $\Delta_0$  in a strong magnetic field. The quasi-classical coupled-orbit model [S14, S15] yields the MB damping factors for the SdH oscillations:  $R_{\text{MB}}^{[\alpha]} = [1 - \exp(-B_0/B)]$  and  $R_{\text{MB}}^{[\beta]} = \exp(-2B_0/B)$ .

spin degeneracy of Landau levels [S11]; hence, the quantum oscillation amplitude has no spin-zeros. The present work extends the validity range of this result from a small Fermi pocket to an arbitrarily large Fermi surface.

## F. DETAILS OF THE SdH FIT FOR $\kappa$ -BETS

In the main text, we noted a large uncertainty of  $B_0$  and  $B_{AF}$ . Here we show that the quality of our SdH amplitude fits is insensitive to the exact values of  $B_0$  and  $B_{AF}$ .

Equation (6) for the amplitude  $A_\delta$  contains the MB factor

$$R_{\text{MB}}^{[\delta]} = \left[ 1 - \exp\left(-\frac{B_0}{B \cos \theta}\right) \right] \left[ 1 - \exp\left(-\frac{B_{AF}}{B \cos \theta}\right) \right], \quad (\text{S7})$$

which must be taken into account when analyzing the angular dependence  $A_\delta(\theta)$ .

A rough estimate of  $B_0$  can be obtained from the SdH oscillation data in the high-field, paramagnetic state [S12], where the SdH spectrum reveals two dominant orbits, shown in Fig. S5: the classical orbit  $\alpha$ , centered at point  $(0, \pm\pi/a)$  on the Brillouin zone boundary – and the MB orbit  $\beta$ , extending beyond the first Brillouin zone. For a magnetic field normal

to the layers, the corresponding oscillation amplitudes  $A_\alpha$  and  $A_\beta$  obtained by Uji et al. [S12] are approximately equal to each other at  $B = 30$  T,  $T = 0.6$  K. To evaluate the relative strength of the oscillations, we use Eq. (6) with the MB factors  $R_{\text{MB}}^{[\alpha]} = [1 - \exp(-B_0/B)]$  and  $R_{\text{MB}}^{[\beta]} = \exp(-2B_0/B)$  for the  $\alpha$  and  $\beta$  oscillations, respectively. Substituting the reported [S12] cyclotron mass values  $m_\alpha = 5.2m_0$  and  $m_\beta = 7.9m_0$  and assuming the Dingle temperature  $T_D = 1$  K, the order of magnitude, typical of organic metals [S16, S17], we obtain a rough estimate  $B_0 \simeq 35$  T. This is an order of magnitude higher than the fields applied to  $\kappa$ -BETS in our experiment. Therefore, the first factor in the right-hand side of Eq. (S7) is close to unity and does not contribute significantly to the angular dependence  $A_\delta(\theta)$ . To confirm this, we have checked how our fits are affected by varying  $B_0$  in the range between 10 T and 50 T, as will be presented below.

The MB field  $B_{\text{AF}}$  is due by magnetic ordering and can be estimated from the gap  $\Delta_{\text{AF}}$  with the help of the Blount criterion [S14, S18],

$$B_{\text{AF}} \sim \frac{m_c}{\hbar e} \cdot \Delta_{\text{AF}}^2 / \varepsilon_F \simeq 0.15 \text{ T}. \quad (\text{S8})$$

Here, we estimated the Fermi energy  $\varepsilon_F$  from SdH oscillations in the paramagnetic state:  $\varepsilon_F \sim \hbar^2 k_F^2 / 2m \sim \hbar e F_\beta / m_{c,\beta}$  with the SdH frequency  $F_\beta = 4280$  T and relevant cyclotron mass  $m_{c,\beta} = 7.9m_0$  [S12].

Of course, these are only rough estimates. Moreover, the observation of the  $\delta$  oscillations in fields up to  $B_c \simeq 5$  T implies that the relevant MB field must be in the range of a few tesla, in order to provide a non-vanishing second factor in the right-hand side of Eq. (S7). On the other hand, the MB field cannot be much higher than the fields we applied ( $B \lesssim B_c$ ), as evidenced by the presence of a small SdH contribution from a bigger orbit,  $F_c \approx 180$  T (see inset in Fig. 2 of the main text), which requires a sufficient MB probability through the AF gap [S19]. Therefore, we have tentatively set the upper estimate for  $B_{\text{AF}}$  at about 5 T and checked how our fits are affected by varying  $B_{\text{AF}}$  from 0.15 T to 5 T.

The results are summarized in Fig.S6, which presents several fits of the experimental data for  $\kappa$ -BETS (the same as in Fig. 3 of the main text), with values of  $B_0$  and  $B_{\text{AF}}$  varying in a broad range:  $10 \text{ T} \leq B_0 \leq 50 \text{ T}$  and  $0.15 \text{ T} \leq B_{\text{AF}} \leq 5 \text{ T}$ . All the fits assume  $g_\perp = 0$ ; as shown in the main text, a finite value for  $g_\perp$  would simply lead to sharp spin-zeros, insensitive to the monotonic  $\theta$ -dependence of  $R_{\text{MB}}$ . One can clearly see that the fits are nearly indistinguishable and virtually insensitive to variation of  $B_0$  within the given range,

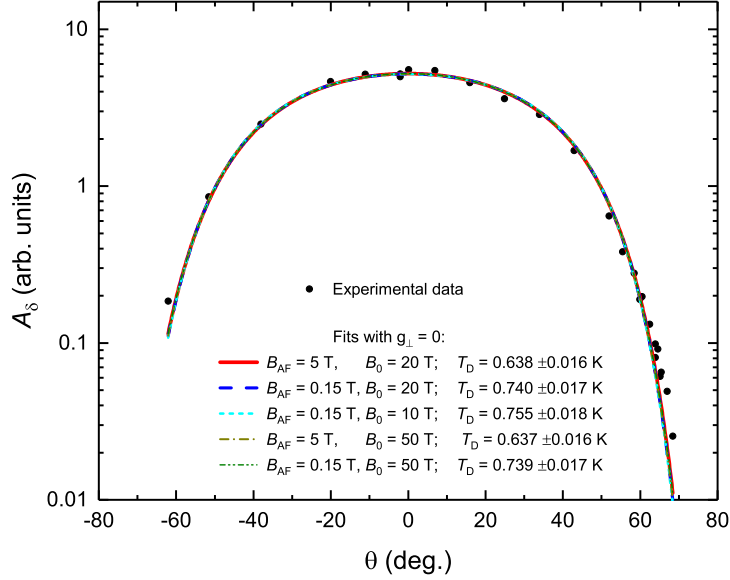


FIG. S6. Fits of the experimental data on the  $\delta$  oscillations in  $\kappa$ -BETS (symbols) to Eq. (5) of the main text, assuming  $g_{\perp} = 0$  and various values for the MB fields  $B_0$  and  $B_{AF}$ , see text. The fit parameters are the angle-independent Dingle temperature  $T_D$  and amplitude prefactor  $A_0$  (not shown).

whereas the variation of  $B_{AF}$  barely results in a 15% change of the Dingle temperature. The parameter  $A_0$  in Eq. (5) changes roughly inversely to  $B_{AF}$ . However,  $A_0$  is largely an empirical parameter, irrelevant to our study. Thus, we conclude that the mentioned uncertainty of the MB fields has no effect on the quality of our fits, as stated in the main text.

- 
- [S1] R. Ramazashvili, Phys. Rev. Lett. **101**, 137202 (2008).  
[S2] R. Ramazashvili, Phys. Rev. B **79**, 184432 (2009).  
[S3] N. P. Armitage, P. Fournier, and R. L. Greene, Rev. Mod. Phys. **82**, 2421 (2010).  
[S4] T. Helm, M. V. Kartsovnik, C. Proust, B. Vignolle, C. Putzke, E. Kampert, I. Sheikin, E.-S. Choi, J. S. Brooks, N. Bittner, W. Biberacher, A. Erb, J. Wosnitza, and R. Gross, Phys. Rev. B **92**, 094501 (2015).  
[S5] J.-F. He, C. R. Rotundu, M. S. Scheurer, Y. He, M. Hashimoto, K. Xu, Y. Wang, E. W. Huang, T. Jia, S.-D. Chen, B. Moritz, D.-H. Lu, Y. S. Lee, T. P. Devereaux, and

- Z.-X. Shen, Proc. Natl. Acad. Sci. USA **116**, 3449 (2019).
- [S6] N. P. Armitage, F. Ronning, D. H. Lu, C. Kim, A. Damascelli, K. M. Shen, D. L. Feng, H. Eisaki, Z.-X. Shen, P. K. Mang, N. Kaneko, M. Greven, Y. Onose, Y. Taguchi, and Y. Tokura, Phys. Rev. Lett. **88**, 257001 (2002).
- [S7] H. Matsui, T. Takahashi, T. Sato, K. Terashima, H. Ding, T. Uefuji, and K. Yamada, Phys. Rev. B **75**, 224514 (2007).
- [S8] N. I. Kulikov and V. V. Tugushev, Sov. Phys. Usp. **27**, 954 (1984).
- [S9] S. A. Brazovskii, I. A. Luk'yanchuk, and R. R. Ramazashvili, JETP Lett. **49**, 644 (1989).
- [S10] V. V. Kabanov, and A. S. Alexandrov, Phys. Rev. B **77**, 132403 (2008); **81**, 099907(E) (2010)
- [S11] R. Ramazashvili, Phys. Rev. B **80**, 054405 (2009).
- [S12] S. Uji, H. Shinagawa, Y. Terai, T. Yakabe, C. Terakura, T. Terashima, L. Balicas, J. S. Brooks, E. Ojima, H. Fujiwara, H. Kobayashi, A. Kobayashi, and M. Tokumoto, Physica B **298**, 557 (2001).
- [S13] H. Fujiwara, E. Fujiwara, Y. Nakazawa, B. Zh. Narymbetov, K. Kato, H. Kobayashi, A. Kobayashi, M. Tokumoto, and P. Cassoux, J. Am. Chem. Soc. **123**, 306 (2001).
- [S14] D. Shoenberg, *Magnetic Oscillations in Metals* (Cambridge University Press, Cambridge, 1984).
- [S15] L. M. Falicov and H. Stachowiak, Phys. Rev. **147**, 505 (1966).
- [S16] J. Wosnitzer, *Fermi Surfaces of Low-Dimensional Organic Metals and Superconductors* (Springer Verlag, Berlin Heidelberg, 1996).
- [S17] M. V. Kartsovnik, Chem. Rev. **104**, 5737 (2004).
- [S18] E. I. Blount, Phys. Rev. **126**, 1636 (1962).
- [S19] T. Konoike, S. Uji, T. Terashima, M. Nishimura, T. Yamaguchi, K. Enomoto, H. Fujiwara, B. Zhang, and H. Kobayashi, J. Low Temp. Phys. **142**, 531 (2006).